Observation of highly disparate *K*-shell x-ray spectra produced by charge exchange with bare mid-*Z* ions

Gabriele L. Betancourt-Martinez,[1,2] Peter Beiersdorfer,[3] Gregory V. Brown,[3] Richard L. Kelley,[2] Caroline A. Kilbourne,[2] Dimitra Koutroumpa,[4] Maurice A. Leutenegger,[2,5] and F. Scott Porter[2]

[1]*CRESST and University of Maryland, College Park, Maryland 20742, USA*
[2]*NASA Goddard Space Flight Center, Greenbelt, Maryland 20771, USA*
[3]*Lawrence Livermore National Laboratory, Livermore, California 94550, USA*
[4]*LATMOS-IPSL/CNRS, Guyancourt, France*
[5]*CRESST and University of Maryland, Baltimore County, Maryland 21250, USA*

(Received 10 June 2014; published 26 November 2014)

We performed charge-exchange experiments with the electron-beam ion trap and an x-ray calorimeter spectrometer at the Lawrence Livermore National Laboratory. We compare the relative strength of the high-n Lyman series emission for different combinations of ions and neutral gases. Theoretical predictions show good agreement with experimental data on the relative capture cross section as a function of principal quantum number n; however, the few published predictions of the distribution of captures as a function of orbital angular momentum l do not agree with experiments. Our experimental results show that the relative strength of high-n Lyman series emission varies more widely than previous experiments have found and models predict. We find that hardness ratios from charge exchange with helium and molecular hydrogen are more disparate than charge exchange with many-electron neutral species, which is likely due to differences in the relative importance of multielectron capture. We also find that there is no clear scaling of the hardness ratio with the ionization potential of the neutral species, the number of valence electrons in the neutral species, or the atomic number of the ion.

DOI: 10.1103/PhysRevA.90.052723 PACS number(s): 34.70.+e, 32.30.Rj, 95.30.Ky, 52.72.+v

I. INTRODUCTION

Charge exchange (CX), or charge transfer, is a semiresonant process in which a highly charged ion captures one or more electrons from a neutral atom or molecule during a close interaction. Charge exchange is important in setting the ionization balance in the laboratory and astrophysical plasmas, as a spectral diagnostic for fusion plasmas, in determining the storage time in ion traps and storage rings, and in antihydrogen production [1–15]. Astrophysically, charge exchange occurs in planetary atmospheres and the comae of comets interacting with the solar wind and has been hypothesized to occur at the rim of supernova remnants [16,17]. Charge exchange also occurs between solar wind ions and neutrals in the exosphere and in the heliosphere, which adds variable foreground emission for every astrophysical observation from our solar system [18–26]. Astro-H, a Japan Aerospace Exploration Agency satellite observatory scheduled for launch in 2015, features an x-ray calorimeter imaging spectrometer that will measure the first high-resolution x-ray spectra of extended objects. Correct interpretation of these observations will require accurate modeling of foreground CX.

In order to model CX spectra, we must know the n- and l-selective electron-capture cross sections. Classical treatment predicts a sharp peak in the n-capture distribution at $n_c \sim q^{3/4}\sqrt{\frac{I_H}{I_n}}$, where I_H and I_n are the ionization potentials of hydrogen and the neutral target, respectively, and q is the ion charge [27]. The n distribution is generally well understood, and many papers show good agreement between theory and experiment for n-selective capture cross sections as in Mawhorter *et al.* [10], Otranto and Olson [28], Igenbergs *et al.* [29], and Wu *et al.* [30].

The l distribution, which is dependent on collision energy, is more challenging to model correctly. One can use classical considerations to determine the electron-capture state: In high-energy collisions, in the limit of strong Stark mixing, l states are assumed to be populated statistically, and high-l states dominate [27]. In low-energy collisions, the electron does not have enough angular momentum to populate the higher-l states, and statistical assumptions do not apply. This was verified in, for example, Beiersdorfer *et al.* [31].

The Lyman (Ly) series x-ray emission is a powerful diagnostic for determining the state-selective capture cross section σ_{nl} in bare ions undergoing charge exchange with a neutral gas. Electron capture into an $l = 1$ state is dominated by direct decay from n_c, $l = 1$ to the ground state [32], emitting a $n_c p \rightarrow 1s$ Ly series photon. If the electron is captured into a high angular momentum state, it will decay along the yrast chain in steps of $\Delta n = -1$ and $\Delta l = -1$, finally yielding a $2p \rightarrow 1s$ Ly α photon. Therefore, if the electrons are captured following a statistical cross section, the strongest line in the spectrum will be Ly α; if the electron-capture cross section is largest for an np state, the $n_c p \rightarrow 1s$ Ly lines will dominate.

The hardness ratio $\mathcal{H}$ is the ratio of the $n_c p \rightarrow 1s$ to $2p \rightarrow 1s$ emission, where n is greater than 2, i.e.,

$$\mathcal{H} = \frac{\sum_{n=3}^{\infty} F_{n\rightarrow 1}}{F_{2\rightarrow 1}}, \tag{1}$$

where F represents the flux in the denoted transition lines. The hardness ratio is expected to decrease with increasing collision energy since as collision energy increases, so does the cross section for capture into higher angular momentum states, producing more Ly α photons. The hardness ratio can

therefore be used as a probe of the collision velocity, allowing us to measure, for example, the velocity of the solar wind. An added benefit of the hardness ratio is that, in principle, it can be determined even with medium-resolution detectors that may not be able to resolve individual high-n Lyman lines, such as CCDs or high-purity germanium solid-state detectors that typically have resolutions on the order of $\sim$100 eV at 1.5 keV.

Besides the classical over-the-barrier (COB) method [33,34], several other more complex charge-exchange models exist which can be used to estimate total or state-selective cross sections. These include the Landau-Zener (LZ) method [35], the multichannel Landau-Zener (MCLZ) approximation [36], the atomic-orbital close-coupling (AOCC) method, and the molecular-orbital close-coupling (MOCC) method [37,38]. The classical trajectory Monte Carlo (CTMC) method [39,40] is the most widely used approximation due to its simplicity and its accuracy compared to other models in predicting experimentally measured n-state selective cross sections.

COB and CTMC models agree qualitatively with experiments that show a decrease in hardness ratios with increasing collision velocity [41]. Both models also agree qualitatively with experiments that show an increase in capture cross section with increasing ion charge but have systematic uncertainties of $\sim$25–50% when predicting absolute cross sections [9,10,42]. CTMC shows better agreement with experiments at high collision energies (above $\sim$1 keV amu^{-1}) as demonstrated in comparison with experimental results from fusion plasmas excited with a very energetic hydrogen or deuterium beam [14]. However, discrepancies between models and experiments arise at the edge of tokamaks where cold ions interact with molecular gas in electron-beam ion traps (EBITs) where the collision velocity is $\sim$10 eV amu^{-1} and in space where cometary, exospheric, and heliospheric neutrals interact with low-energy solar wind ions.

The COB and LZ methods do not make predictions for l-selective capture cross sections, and to the extent that there are measurements of l-selective capture cross sections at low collision energies, especially over a range of conditions and interacting species other than atomic hydrogen, theoretical calculations that can incorporate l, such as CTMC, AOCC, and MOCC, show poor agreement with experiments [30,31,43–45]. Furthermore, the commonly used CTMC method cannot incorporate multielectron capture (MEC), which becomes important in the low-energy regime [41,46].

Several comparisons between theory and experiment have been made with varying results. Otranto *et al.* [41] demonstrated that, although CTMC calculations qualitatively agree with EBIT experiments where n_c decreases for increasing ionization potential, their CTMC model overestimates the flux in high-n Rydberg transitions following CX onto O^{8+}. Beiersdorfer *et al.* [31] performed experiments with EBIT-I showing that, contrary to CTMC calculations, the hardness ratio following CX with bare Ne, Ar, Kr, and Xe was always nearly unity. Furthermore, the disagreement between calculated and measured hardness ratios worsened at higher atomic numbers. Otranto *et al.* [47] presented EBIT results involving O^{8+} demonstrating that the hardness ratio can vary within nearly a factor of 2 by varying the neutral gas. Leutenegger *et al.* [43] presented EBIT spectra of bare Ar and P that concurrently underwent CX with the same neutral gas, and contrary to the trend established in Ref. [31] and to previous CTMC calculations, the hardness ratios measured for Ar and P differed by a factor of 2.

In this paper, we present experiments that investigate the dependence of CX line emission on the ionization potential of the neutral gas, the number of valence electrons in the neutral gas, and the atomic number of the ion. We probe whether any of these characteristics are predictive of CX spectral features and provide empirical data towards more comprehensive and quantitatively accurate models.

II. EXPERIMENTAL METHOD

The measurements presented here were performed with the EBIT-I electron-beam ion trap at the Lawrence Livermore National Laboratory [48,49]. The spectra were measured using the EBIT calorimeter spectrometer (ECS) [50,51]. The ECS is a nondispersive spectrometer developed at the NASA-Goddard Space Flight Center with quantum efficiency of nearly unity over a large bandwidth. The 30-pixel array of silicon-doped thermistors is divided into a mid- and a high-energy array of 16 and 14 pixels, respectively, which together have a dynamic range of 0.05–100 keV. The experiments discussed here made use of the midband array, which has an energy resolution of $\sim$4.5 eV at 6 keV.

The ECS has four internal aluminized polyimide filters used to block optical and thermal radiation at temperature stages of 77, 4 K, 300, and 50 mK with a total aluminum thickness of 1460 Å and a total polyimide thickness of 2380 Å. In addition, we used a 500-Å polyimide window outside the ECS dewar to isolate the ECS vacuum from the EBIT vacuum. These thicknesses have been experimentally verified to an accuracy of $\sim$10%.

Fundamentally, the EBIT operates in one of two modes: the electron trapping mode and the magnetic trapping mode. In the electron trapping mode, after neutral species are injected into the ion trap, they are collisionally ionized by the electron beam then confined in the trap. The ions are radially confined due to the electrostatic attraction of the electron beam and axially confined by a voltage potential applied across three copper drift tubes. Typical thermal energies of trapped ions are $\sim$10 eV amu^{-1} at typical beam currents of $\geqslant$130 mA and trap potentials of $\geqslant$ 100 V [52], and typical ion densities in the trap are $\sim 3\times 10^9$ cm^{-3}.

For a charge-exchange experiment in the EBIT-I, first, ions are created during the electron trapping mode with the electron beam turned on for typically about 0.5 s to generate a sufficient number of bare ions of mid-Z elements. Next, in the magnetic trapping mode [53], the electron beam is turned off, and the ions are radially trapped by the 3-T magnetic field of the superconducting Helmholtz coils and the electric field of the drift tubes so that the EBIT is effectively a Penning trap. The ions gain electrons and emit x rays through CX with the neutral species introduced into the trap. Since the beam is off, no excitations due to electron impact occur. Filling the K shell of most of the trapped bare ions takes about 0.5 s. After this occurs, the trap is dumped, and the cycle is repeated.

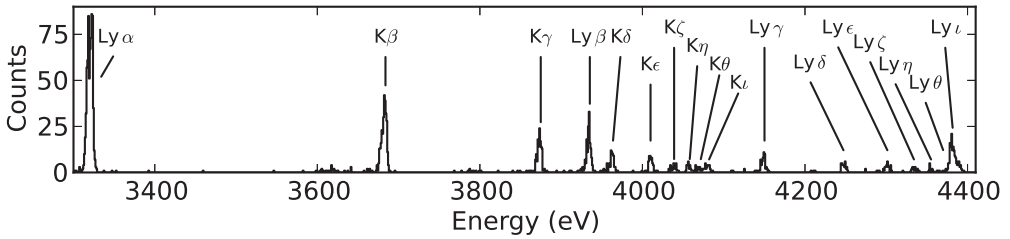

FIG. 1. Spectrum of bare argon undergoing CX with neutral argon.

It typically requires several hours to accumulate sufficient statistics for each experiment.

We performed charge-exchange experiments for the following ions and neutral gases: $Mg^{12+} + CO_2$, $Mg^{12+} + H_2$, $Mg^{12+} + He$, $Mg^{12+} + Ne$, $Cl^{17+} + C_2H_4Cl_2$, $Cl^{17+} + He$, $Ar^{18+} + Ar$, $S^{16+} + He$, and $S^{16+} + SF_6$. In the Mg experiments, there were contaminant ions present in the trap, including P, S, Si, and Ar, which entered from a port on the EBIT that was open in order to perform crystal spectrometer measurements. We did not observe any significant effect from these contaminants in the spectra, other than the presence of their K-shell emission lines. The charge-exchange cross section for ion-ion interactions is negligible. We verified that the x rays recorded were nearly all from interactions of trapped ions with the chosen neutral gas and not with background gases in the trap by reducing the neutral CX partner gas injection pressure to zero while holding all other experimental parameters constant. From contemporaneous measurements, we estimate that the background CX rate for the Mg experiments was about 10% of the experimental CX rate; for all other experiments the background rate is on the order of 1%.

III. ANALYSIS AND SPECTRA

We fit Lyman series lines from H-like ions, assuming a Gaussian instrumental function [54]. We used reference energies calculated with the Flexible Atomic Code [55]. We accounted for partial line blending where two transitions from different ions could be disentangled due to differing energy centroids. In a few cases, however, ion line flux could not be separated from other lines due to contaminants with transitions that overlapped with the lines of interest: for example, Mg^{11+} Ly γ is nearly coincident with the strong $Si^{12+} 1s2s\ ^3S_1 \rightarrow 1s^2\ ^1S_0$ transition. In order to account for this in our hardness ratios, we determined a lower limit assuming zero flux in Ly γ, which appears in the text of Table I and Figs. 4 and 5, and an upper limit by including the entire blended line, mentioned in the caption of Table I. In the absence

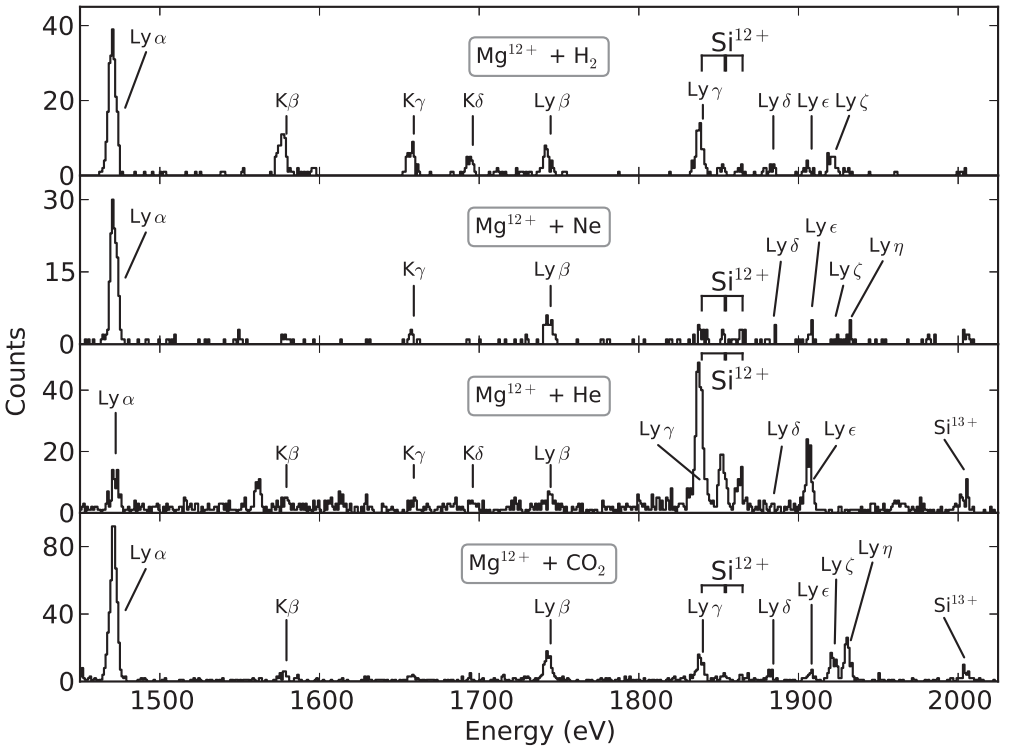

FIG. 2. Spectra from bare Mg undergoing CX with four different neutral gases. Relevant transitions along with background ions are labeled.

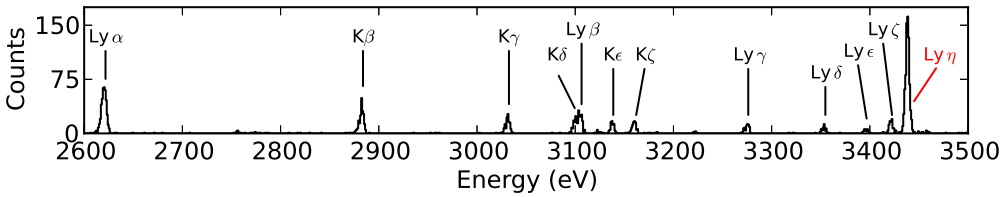

FIG. 3. (Color online) Spectrum from charge exchange between S^{16+} and He. Note the extremely strong $8 \rightarrow 1$ transition (Ly η) identified in red.

of independent measurements of the Si lines, we assert that the lower limit is the more realistic one; the Si forbidden line in CX is more likely to be stronger than the Mg^{11+} Ly γ line.

We corrected the observed flux for attenuation from the optical and thermal blocking filters as well as frozen contaminants on the filters, which we believe is either or both of water ice or nitrogen gas frozen on the 77-K filter or nitrogen gas frozen on the 4-K filter. Since the photoelectric absorption cross section scales very nearly as E^{-3}, either substance would produce the same transmission curve at energies above the oxygen K threshold, assuming a given optical depth at a given energy. Therefore, we make a fiducial assumption that the contaminant is water ice. We determine the thickness of water ice using the decrement in the ratio of the O Ly α to Ly β line strengths in electron impact excitation experiments compared to the measured ratio of 6.25 in the limit of high incident electron-beam energy [56]. The oxygen measurements were taken regularly during the experiments. The inferred fiducial ice layer thickness was typically ~ 1 μm, which corresponds to a line flux correction of $\sim$10–20% in the Mg Ly band from 1300 to 1900 eV and $\sim$1% for the S, Cl, and Ar experiments with line energies above $\sim$2400 eV. This corresponds to a maximum effect on the ratio of Ly n:Ly α of $\sim$10% for the Mg experiments and $\sim$1% for the S, Cl, and Ar experiments.

Selected spectra are presented in Figs. 1–3. Lyman lines refer to the hydrogenlike ion emission; K lines refer to He-like ion emission. K lines can be used for various diagnostics, but in this paper we focus on the Lyman emission. Hardness ratios and other diagnostic ratios for all experiments are summarized in Tables I and II in the Appendix. Individual line fluxes are also presented in the Appendix.

IV. DISCUSSION

The hardness ratios determined for the experiments presented here span a larger range than previous experiments have shown and can deviate widely from CTMC calculations as can be seen in Fig. 4. In earlier CX experiments using trapped ions, the hardness ratio measured at low collision velocity was often ~ 1 [31,41,57–60]. All experiments in this paper were performed at similar collision energies of $\lesssim$25 eV amu^{-1} [56], but the hardness ratios vary between $\sim$0.5 and $\sim$2.6. This demonstrates that the contribution from the np-capture cross section as normalized to the total capture cross section occupies a broader range than previously supposed; the initially surprising variation in $\mathcal{H}$ between bare Ar and P as shown in Ref. [43] seems to be less of an anomaly than formerly thought.

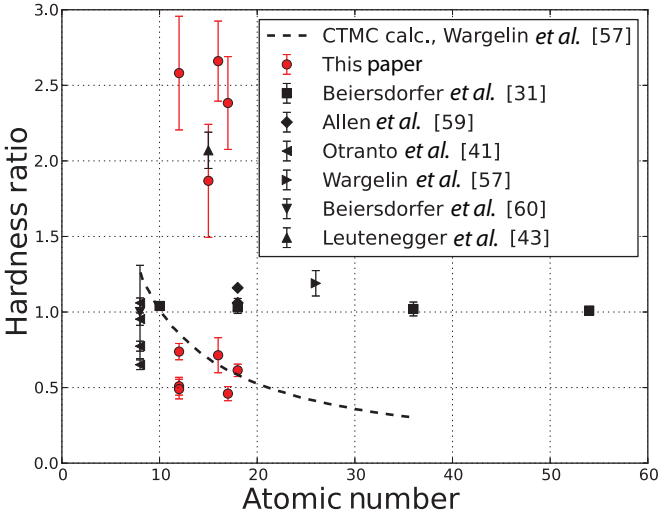

FIG. 4. (Color online) Hardness ratio as a function of the atomic number of the ion. All experiments were performed at less than $\sim$25 eV amu^{-1}.

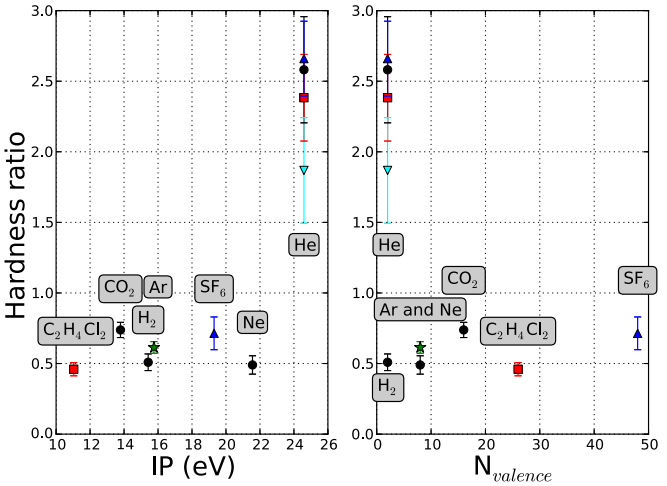

FIG. 5. (Color online) Hardness ratio as a function of the ionization potential (left) and the number of valence electrons (right) of the neutral gas. Colors and symbols represent different bare ions: Mg in black circles, Cl in red squares, Ar in green stars, S in blue upward-pointing triangles, and P in cyan downward-pointing triangles. The neutral species is indicated on the plot.

One might expect to see $\mathcal{H}$ scale with the atomic number of the ion (as CTMC calculations in Refs. [31,32] show), the number of valence electrons in the neutral ion, or the ionization potential of the neutral ion. For example, Ali *et al.* [61] notes that single electron capture (SEC) from a neutral ion with a large ionization potential would require a smaller impact parameter, leading to a low-l state of the captured electron. However, our results also show that there is no clear scaling between the l distribution of captures and any of the aforementioned parameters as can be seen in Figs. 4 and 5.

The fact that we do not see a scaling of $\mathcal{H}$ with the ionization potential in particular may stem from the relative dominance of SEC versus MEC. As pointed out by Ali *et al.* [61], MEC produces multiply charged ions that autoionize until reaching a lower n,l state that radiatively decays. This leads to fewer high-n Lyman lines and thus a smaller $\mathcal{H}$. In our experiments, we find that charge exchange with helium as the neutral partner shows an especially high $\mathcal{H}$. This is likely due to a high percentage of single electron capture as Ali *et al.* [61] demonstrated in addition to the high ionization potential of He. However, we measure a low $\mathcal{H}$ ($\sim$0.5) for experiments with molecular H, even though one would expect SEC to be dominant for H_2.

We suggest that in the case of SEC, the differences we measure in hardness ratio from CX with otherwise similar neutrals stem from inherent differences in the np-cross section of those species. These differences can likely only be understood in the context of a rigorous quantum-mechanical treatment of the interaction, which must be guided by further experimental benchmarks.

The large variation in hardness ratio we have shown from charge-exchange experiments performed at low collision energies in comparison with both previous papers in the literature and theoretical calculations using models, such as CTMC, demonstrates that open questions still exist in determining the l-selective CX capture cross section distribution and therefore the resulting x-ray spectrum and its accompanying diagnostics. This is an issue that is imperative to address now, so as to properly interpret the high-resolution spectra from the Astro-H x-ray satellite observatory and high-resolution x-ray microcalorimeters to be implemented on future space missions.

ACKNOWLEDGMENTS

The authors would like to thank E. Magee and D. Layne at LLNL for their technical support. We also thank the anonymous referees for their helpful comments. Work at the Lawrence Livermore National Laboratory was performed under the auspices of the U.S. Department of Energy under Contract No. DE-AC52-07NA27344 and was supported by NASA APRA grants to LLNL and NASA-GSFC.

APPENDIX: RATIOS AND INDIVIDUAL LINE STRENGTHS

Hardness ratios, other diagnostic ratios, and individual line fluxes for all experiments are summarized in Tables I and II.

TABLE I. This table summarizes the normalized H-like series line strengths and hardness ratios for the experiments presented in the text. Filter transmission- and ice-corrected line strengths are normalized to the sum of Ly-α 1 and 2. Uncertainties are 1σ statistical errors. The flux ratio for Ly-α 1:2 was set to 2 in the model fits for the Mg experiments, but for the other experiments, this ratio was allowed to vary and is presented in the table. The line strengths listed for the Mg^{12+} Ly-γ lines are upper limits, including both the flux in the Mg Ly-γ line as well as the $Si^{12+}1s2s^3S_1 \rightarrow 1s^2\,{}^1S_0$ overlapping transition. The hardness ratios listed for the Mg^{12+} experiments are calculated assuming the lower limit, i.e., zero flux in this blended Mg Ly-γ line. The upper limits on $\mathcal{H}$, which use the upper limit flux in Ly γ, are the following: $Mg^{12+} + CO_2$: 0.905 $\pm$ 0.063, Mg^{12+} + He: 6.446 $\pm$ 0.832, $Mg^{12+} + H_2$: 0.846 $\pm$ 0.087, Mg^{12+} + Ne: 0.623 $\pm$ 0.076.

Transition	$Mg^{12+} + CO_2$	Mg^{12+} + He	$Mg^{12+} + H_2$	Mg^{12+} + Ne	P^{15+} + He	S^{16+} + He	$S^{16+} + SF_6$	Cl^{17+} + He	$Cl^{17+} + C_2H_4Cl_2$	Ar^{18+} + Ar
1s-3p	0.211 $\pm$ 0.022	0.610 $\pm$ 0.099	0.184 $\pm$ 0.033	0.227 $\pm$ 0.040	0.281 $\pm$ 0.075	0.32 $\pm$ 0.12	0.203 $\pm$ 0.070	0.239 $\pm$ 0.050	0.227 $\pm$ 0.030	0.204 $\pm$ 0.020
1s-4p	0.167 $\pm$ 0.020	3.86 $\pm$ 0.28	0.337 $\pm$ 0.044	0.133 $\pm$ 0.022	0.285 $\pm$ 0.076	0.155 $\pm$ 0.022	0.082 $\pm$ 0.016	0.253 $\pm$ 0.051	0.066 $\pm$ 0.014	0.084 $\pm$ 0.012
1s-5p	0.058 $\pm$ 0.011	0.319 $\pm$ 0.073	0.063 $\pm$ 0.011	0.044 $\pm$ 0.015	0.210 $\pm$ 0.057	0.114 $\pm$ 0.019	0.053 $\pm$ 0.011	0.150 $\pm$ 0.034	0.0399 $\pm$ 0.0052	0.0528 $\pm$ 0.0091
1s-6p	0.064 $\pm$ 0.012	1.41 $\pm$ 0.16	0.063 $\pm$ 0.012	0.095 $\pm$ 0.015	0.120 $\pm$ 0.032	0.069 $\pm$ 0.013	0.0527 $\pm$ 0.0082	0.078 $\pm$ 0.015	0.0449 $\pm$ 0.0059	0.0466 $\pm$ 0.0087
1s-7p	0.169 $\pm$ 0.020	0.053 $\pm$ 0.043	0.146 $\pm$ 0.026	0.030 $\pm$ 0.018	0.82 $\pm$ 0.18	0.213 $\pm$ 0.028	0.0162 $\pm$ 0.0050	0.037 $\pm$ 0.017	0.0249 $\pm$ 0.0056	0.0272 $\pm$ 0.0042
1s-8p	0.229 $\pm$ 0.024	0.072 $\pm$ 0.039	0.036 $\pm$ 0.014	0.080 $\pm$ 0.014	0.092 $\pm$ 0.036	1.74 $\pm$ 0.14	0.0291 $\pm$ 0.0078	1.60 $\pm$ 0.22	0.0262 $\pm$ 0.0064	0.0169 $\pm$ 0.0040
1s-9p	0.0054 $\pm$ 0.0078	0.074 $\pm$ 0.052	0.0133 $\pm$ 0.0050	0.0084 $\pm$ 0.0041	0.059 $\pm$ 0.029	0.0125 $\pm$ 0.0089	0.111 $\pm$ 0.019	0.026 $\pm$ 0.026	0.0184 $\pm$ 0.0072	0.0016 $\pm$ 0.0039
1s-10p	0.0028 $\pm$ 0.0054	0.048 $\pm$ 0.052	0.0031 $\pm$ 0.0063	0.0059 $\pm$ 0.0090	0.003 $\pm$ 0.013	0.0330 $\pm$ 0.0062	0.165 $\pm$ 0.024	0.0001 $\pm$ 0.0097	0.0130 $\pm$ 0.0099	0.181 $\pm$ 0.019
Ly-α 1:2						2.19 $\pm$ 0.36	2.22 $\pm$ 0.45	1.16 $\pm$ 0.27	1.26 $\pm$ 0.19	1.41 $\pm$ 0.19
$\mathcal{H}$	0.738 $\pm$ 0.054	2.581 $\pm$ 0.376	0.509 $\pm$ 0.059	0.490 $\pm$ 0.065	1.868 $\pm$ 0.374	2.660 $\pm$ 0.265	0.714 $\pm$ 0.116	2.383 $\pm$ 0.307	0.460 $\pm$ 0.047	0.614 $\pm$ 0.041

TABLE II. This table presents the normalized He-like series line strengths for the experiments presented in the text except for $Mg^{11+}+Ne$, which had significant line blending in the Mg forbidden (z), intercombnation (y and x), and resonance (w) lines with Ne^{9+}. Filter transmission- and ice-corrected line strengths are normalized to w. Uncertainties are 1σ statistical errors. Also presented are the He-like line ratios defined in Ref. [62]: $\mathcal{R} = F_z/(F_x + F_y)$, $\mathcal{G} = F_x + F_y + F_z/F_w$, an alternate quantity giving the triplet-to-singlet capture ratio $\mathcal{G}' = (F_x + F_y + F_z)/(F_w + F_{3+})$, the He-like hardness ratio $\mathcal{H} = F_{3+}/(F_2)$, and a ratio introduced in Ref. [43], $\mathcal{H}' = F_{3+}/F_w$. F represents the flux in the denoted transition lines.

Transition	$Mg^{11+} + CO_2$	$Mg^{11+} + He$	$Mg^{11+} + H_2$	$S^{15+} + He$	$S^{15+} + SF_6$	$Cl^{16+} + He$	$Cl^{16+} + C_2H_4Cl_2$	$Ar^{17+} + Ar$
z	1.53 ± 0.16	3.71 ± 0.59	2.90 ± 0.24	5.12 ± 0.25	1.60 ± 0.12	5.82 ± 0.38	1.520 ± 0.096	1.889 ± 0.084
x/y	1.23 ± 0.14	1.28 ± 0.24	0.861 ± 0.092	1.777 ± 0.098	1.61 ± 0.12	2.23 ± 0.21	1.65 ± 0.14	1.39 ± 0.18
$1s$-$3p$	0.219 ± 0.043	0.71 ± 0.16	0.347 ± 0.051	0.349 ± 0.030	0.231 ± 0.031	0.450 ± 0.051	0.185 ± 0.024	0.296 ± 0.022
$1s$-$4p$	0.184 ± 0.040	0.56 ± 0.14	0.209 ± 0.036	0.216 ± 0.023	0.117 ± 0.021	0.307 ± 0.038	0.107 ± 0.018	0.135 ± 0.014
$1s$-$5p$	0.108 ± 0.024	0.47 ± 0.11	0.125 ± 0.026	0.176 ± 0.026	0.065 ± 0.023	0.141 ± 0.023	0.062 ± 0.013	0.076 ± 0.010
$1s$-$6p$	0.090 ± 0.024	0.145 ± 0.086	0.030 ± 0.011	0.141 ± 0.018	0.0411 ± 0.0059	0.112 ± 0.022	0.0440 ± 0.0089	0.0616 ± 0.0092
$1s$-$7p$	0.114 ± 0.029	0.42 ± 0.12	0.029 ± 0.012	0.160 ± 0.019	0.0152 ± 0.0061	0.220 ± 0.033	0.0212 ± 0.0047	0.0290 ± 0.0057
$1s$-$8p$		0.315 ± 0.098	0.018 ± 0.018	0.0050 ± 0.0053	0.0244 ± 0.0078	0.0669 ± 0.0095	0.0137 ± 0.0047	0.0287 ± 0.0060
$1s$-$9p$				0.0055 ± 0.0042	0.0293 ± 0.0077	0.0002 ± 0.0033	0.0029 ± 0.0037	0.0195 ± 0.0049
$1s$-$10p$				0.0026 ± 0.0015	0.0012 ± 0.0041	0.0097 ± 0.0028	0.0140 ± 0.0046	0.0327 ± 0.0061
$\mathcal{R}$	1.248 ± 0.126	2.904 ± 0.420	3.365 ± 0.302	2.879 ± 0.110	0.994 ± 0.064	2.604 ± 0.200	0.922 ± 0.075	1.362 ± 0.179
$\mathcal{G}$	2.755 ± 0.269	4.991 ± 0.777	3.758 ± 0.306	6.893 ± 0.325	3.214 ± 0.215	8.053 ± 0.532	3.169 ± 0.204	3.276 ± 0.218
$\mathcal{G}'$	1.606 ± 0.129	1.378 ± 0.139	2.137 ± 0.143	3.354 ± 0.121	2.108 ± 0.122	3.491 ± 0.168	2.187 ± 0.127	1.857 ± 0.082
$\mathcal{H}$	0.191 ± 0.020	0.438 ± 0.048	0.159 ± 0.015	0.134 ± 0.010	0.124 ± 0.017	0.144 ± 0.008	0.108 ± 0.009	0.159 ± 0.013
$\mathcal{H}'$	0.715 ± 0.091	2.622 ± 0.448	0.759 ± 0.085	1.055 ± 0.090	0.525 ± 0.078	1.307 ± 0.105	0.449 ± 0.040	0.678 ± 0.053

[1] R. C. Isler, Phys. Rev. Lett. **38**, 1359 (1977).
[2] R. J. Fonck, M. Finkenthal, R. J. Goldston, D. L. Herndon, R. A. Hulse, R. Kaita, and D. D. Meyerhofer, Phys. Rev. Lett. **49**, 737 (1982).
[3] R. J. Fonck and R. A. Hulse, Phys. Rev. Lett. **52**, 530 (1984).
[4] E. Källne, J. Källne, A. Dalgarno, E. S. Marmar, J. E. Rice, and A. K. Pradhan, Phys. Rev. Lett. **52**, 2245 (1984).
[5] J. E. Rice, E. S. Marmar, J. L. Terry, E. Kallne, and J. Kallne, Phys. Rev. Lett. **56**, 50 (1986).
[6] T. Stöhlker, T. Ludziejewski, H. Reich, F. Bosch, R. W. Dunford, J. Eichler, B. Franzke, C. Kozhuharov, G. Menzel, P. H. Mokler *et al.*, Phys. Rev. A **58**, 2043 (1998).
[7] G. Gabrielse, P. Larochelle, D. Le Sage, B. Levitt, W. S. Kolthammer, I. Kuljanishvili, R. McConnell, J. Wrubel, F. M. Esser, H. Glückler *et al.* (ATRAP Collaboration), Phys. Rev. Lett. **98**, 113002 (2007).
[8] J. B. Greenwood, I. D. Williams, S. J. Smith, and A. Chutjian, Phys. Rev. A **63**, 062707 (2001).
[9] I. Cadez, J. B. Greenwood, J. Lozano, R. J. Mawhorter, M. Niimura, S. J. Smith, and A. Chutjian, J. Phys. B: At., Mol. Opt. Phys. **36**, 3303 (2003).
[10] R. J. Mawhorter, A. Chutjian, T. E. Cravens, N. Djurić, S. Hossain, C. M. Lisse, J. A. MacAskill, S. J. Smith, J. Simcic, and I. D. Williams, Phys. Rev. A **75**, 032704 (2007).
[11] J. B. Greenwood, R. J. Mawhorter, I. Cadez, J. Lozano, S. J. Smith, and A. Chutjian, Phys. Scr. **T110**, 358 (2004).
[12] J. Simcic, D. R. Schultz, R. J. Mawhorter, I. Čadež, J. B. Greenwood, A. Chutjian, C. M. Lisse, and S. J. Smith, Phys. Rev. A **81**, 062715 (2010).
[13] P. G. Carolan, B. P. Duval, A. R. Field, S. J. Fielding, N. C. Hawkes, N. J. Peacock, G. Fussmann, G. Janeschitz, J. Hofmann, K. H. Behringer *et al.*, Phys. Rev. A **35**, 3454 (1987).
[14] P. Beiersdorfer, M. Bitter, M. Marion, and R. E. Olson, Phys. Rev. A **72**, 032725 (2005).
[15] R. C. Isler, Plasma Phys., Controlled Fusion **36**, 171 (1994).
[16] S. Katsuda, H. Tsunemi, K. Mori, H. Uchida, H. Kosugi, M. Kimura, H. Nakajima, S. Takakura, R. Petre, J. W. Hewitt *et al.*, Astrophys. J. **730**, 24 (2011).
[17] R. S. Cumbee, D. B. Henley, P. C. Stancil, R. L. Shelton, J. L. Nolte, Y. Wu, and D. R. Schultz, Astrophys. J. Lett. **787**, L31 (2014).
[18] C. M. Lisse, K. Dennerl, J. Englhauser, M. Harden, F. E. Marshall, M. J. Mumma, R. Petre, J. P. Pye, M. J. Ricketts, J. Schmitt *et al.*, Science **274**, 205 (1996).
[19] T. E. Cravens, Geophys. Res. Lett. **24**, 105 (1997).
[20] G. R. Gladstone, J. H. Waite, D. Grodent, W. S. Lewis, F. J. Crary, R. F. Elsner, M. C. Weisskopf, T. Majeed, J.-M. Jahn, A. Bhardwaj *et al.*, Nature **415**, 1000 (2002).
[21] K. Dennerl, C. M. Lisse, A. Bhardwaj, V. Burwitz, J. Englhauser, H. Gunell, M. Holmström, F. Jansen, V. Kharchenko, and P. M. Rodríguez-Pascual, Astron. Astrophys. **451**, 709 (2006).
[22] D. Koutroumpa, R. Lallement, V. Kharchenko, and A. Dalgarno, Space Sci. Rev. **143**, 217 (2009).
[23] K. Dennerl, C. M. Lisse, A. Bhardwaj, D. J. Christian, S. J. Wolk, D. Bodewits, T. H. Zurbuchen, M. Combi, and S. Lepri, Astron. Nachr. **333**, 324 (2012).
[24] A. Bhardwaj, R. F. Elsner, G. Randall Gladstone, T. E. Cravens, C. M. Lisse, K. Dennerl, G. Branduardi-Raymont, B. J. Wargelin, J. Hunter Waite, I. Robertson *et al.*, Planet. Space Sci. **55**, 1135 (2007).
[25] T. G. Slanger, T. E. Cravens, J. Crovisier, S. Miller, and D. F. Strobel, Space Sci. Rev. **139**, 267 (2008).
[26] D. Bodewits, Ph.D. thesis, University of Groningen, 2007.
[27] R. K. Janev and H. Winter, Phys. Rep. **117**, 265 (1985).
[28] S. Otranto and R. E. Olson, J. Phys. B: At., Mol. Opt. Phys. **43**, 144004 (2010).
[29] K. Igenbergs, J. Schweinzer, A. Veiter, L. Perneczky, E. Frühwirth, M. Wallerberger, R. E. Olson, and F. Aumayr, J. Phys. B: At., Mol. Opt. Phys. **45**, 065203 (2012).
[30] Y. Wu, P. C. Stancil, D. R. Schultz, Y. Hui, H. P. Liebermann, and R. J. Buenker, J. Phys. B: At., Mol. Opt. Phys. **45**, 235201 (2012).
[31] P. Beiersdorfer, R. E. Olson, G. V. Brown, H. Chen, C. L. Harris, P. A. Neill, L. Schweikhard, S. B. Utter, and K. Widmann, Phys. Rev. Lett. **85**, 5090 (2000).
[32] B. J. Wargelin, P. Beiersdorfer, and G. V. Brown, Can. J. Phys. **86**, 151 (2008).
[33] H. Ryufuku, K. Sasaki, and T. Watanabe, Phys. Rev. A **21**, 745 (1980).
[34] A. Niehaus, J. Phys. B: At., Mol. Phys. **19**, 2925 (1986).
[35] A. Salop and R. E. Olson, Phys. Rev. A **13**, 1312 (1976).
[36] R. K. Janev, D. S. Belić, and B. H. Bransden, Phys. Rev. A **28**, 1293 (1983).
[37] W. Fritsch and C. D. Lin, Phys. Rep. **202**, 1 (1991).
[38] N. Shimakura, S. Suzuki, and M. Kimura, Phys. Rev. A **48**, 3652 (1993).
[39] R. Abrines and I. C. Percival, Proc. Phys. Soc. **88**, 861 (1966).
[40] R. E. Olson and A. Salop, Phys. Rev. A **16**, 531 (1977).
[41] S. Otranto, R. E. Olson, and P. Beiersdorfer, Phys. Rev. A **73**, 022723 (2006).
[42] N. Djurić, S. J. Smith, J. Simcic, and A. Chutjian, Astrophys. J. **679**, 1661 (2008).
[43] M. A. Leutenegger, P. Beiersdorfer, G. V. Brown, R. L. Kelley, C. A. Kilbourne, and F. S. Porter, Phys. Rev. Lett. **105**, 063201 (2010).
[44] P. C. Stancil, J. G. Wang, M. J. Rakovic, D. R. Schultz, and R. Ali, in *Atomic and Molecular Data and Their Applications*, edited by D. R. Schultz, P. S. Krstic, and F. Ownby, AIP Conf. Proc. No. 636 (AIP, New York, 2002), pp. 144–153.
[45] I. Mančev, N. Milojević, and D. Belkić, Phys. Rev. A **88**, 052706 (2013).
[46] R. Ali, C. L. Cocke, M. L. A. Raphaelian, and M. Stockli, Phys. Rev. A **49**, 3586 (1994).
[47] S. Otranto, R. E. Olson, and P. Beiersdorfer, J. Phys.: Conf. Ser. **58**, 165 (2007).
[48] P. Beiersdorfer, E. Behar, K. R. Boyce, G. V. Brown, H. Chen, K. C. Gendreau, A. Graf, M.-F. Gu, C. L. Harris, S. M. Kahn *et al.*, Nucl. Instrum. Methods Phys. Res., Sect. B **205**, 173 (2003).
[49] P. Beiersdorfer, Can. J. Phys. **86**, 1 (2008).
[50] F. S. Porter, G. V. Brown, K. R. Boyce, R. L. Kelley, C. A. Kilbourne, P. Beiersdorfer, H. Chen, S. Terracol, S. M. Kahn, and A. E. Szymkowiak, Rev. Sci. Instrum. **75**, 3772 (2004).
[51] F. S. Porter, B. R. Beck, P. Beiersdorfer, K. R. Boyce, G. V. Brown, H. Chen, J. Gygax, S. M. Kahn, R. L. Kelley, C. A. Kilbourne *et al.*, Can. J. Phys. **86**, 231 (2008).

[52] P. Beiersdorfer, A. L. Osterheld, V. Decaux, and K. Widmann, Phys. Rev. Lett. **77**, 5353 (1996).
[53] P. Beiersdorfer, L. Schweikhard, J. Crespo López-Urrutia, and K. Widmann, Rev. Sci. Instrum. **67**, 3818 (1996).
[54] R. L. Kelley, K. Mitsuda, C. A. Allen, P. Arsenovic, M. D. Audley, T. G. Bialas, K. R. Boyce, R. F. Boyle, S. R. Breon, G. V. Brown *et al.*, Publ. Astron. Soc. Jpn. **59**, S77 (2007).
[55] M. F. Gu, Can. J. Phys. **86**, 675 (2008).
[56] P. Beiersdorfer, Annu. Rev. Astron. Astrophys. **41**, 343 (2003).
[57] B. J. Wargelin, P. Beiersdorfer, P. A. Neill, R. E. Olson, and J. H. Scofield, Astrophys. J. **634**, 687 (2005).
[58] M. A. Leutenegger, G. L. Betancourt-Martinez, P. Beiersdorfer, G. V. Brown, R. L. Kelley, C. A. Kilbourne, and F. S. Porter, Phys. Scr. **T156**, 014006 (2013).
[59] F. I. Allen, C. Biedermann, R. Radtke, G. Fussmann, and S. Fritzsche, Phys. Rev. A **78**, 032705 (2008).
[60] P. Beiersdorfer, C. M. Lisse, R. E. Olson, G. V. Brown, and H. Chen, Astrophys. J. Lett. **549**, L147 (2001).
[61] R. Ali, P. A. Neill, P. Beiersdorfer, C. L. Harris, M. J. Raković, J. G. Wang, D. R. Schultz, and P. C. Stancil, Astrophys. J. Lett. **629**, L125 (2005).
[62] A. H. Gabriel and C. Jordan, Mon. Not. R. Astron. Soc. **145**, 241 (1969).